INTERNATIONAL ATOMIC ENERGY AGENCY **INDC(CCP)-417**
Distr. L0+FE

I N D C **INTERNATIONAL NUCLEAR DATA COMMITTTEE**

BENCHMARKING OF EVALUATED NEUTRON DATA FOR VANADIUM BY A 14 MEV SPHERICAL SHELL TRANSMISSION EXPERIMENT

Final Report of Research Contract 9268

S.P. Simakov, B.V. Devkin, B.I. Fursov, M.G. Kobozev, V.A.Talalaev
Institute of Physics and Power Engineering
Obninsk, Russia

U. von Möllendorff
Forschungszentrum Karlsruhe,
Institut für Neutronenphysik und Reaktortechnik
Karlsruhe, Germany

M.M. Potapenko
Institute of Inorganic Materials
Moscow, Russia

October 1998

Reproduced by the IAEA in Austria

October 1998

INDC(CCP)-417
Distr. L0+FE

BENCHMARKING OF EVALUATED NEUTRON DATA FOR VANADIUM BY A 14 MEV SPHERICAL SHELL TRANSMISSION EXPERIMENT

Final Report of Research Contract 9268

S.P. Simakov, B.V. Devkin, B.I. Fursov, M.G. Kobozev, V.A.Talalaev
Institute of Physics and Power Engineering
Obninsk, Russia

U. von Möllendorff
Forschungszentrum Karlsruhe,
Institut für Neutronenphysik und Reaktortechnik
Karlsruhe, Germany

M.M. Potapenko
Institute of Inorganic Materials
Moscow, Russia

Abstract

Measurements of neutron leakage spectra from two shells of pure vanadium having wall thicknesses of 3.5 cm and 10.5 cm with a 14 MeV neutron source at the center are reported. The neutron leakage spectra were measured by the time-of-flight method from 15 MeV down to 50 keV. Descriptions of the experimental arrangement, the time-of-flight spectrometer, the measurements and data reduction procedures are given. Corrections connected with neutron multiple scattering in the neutron source, deviations from spherical symmetry and others were estimated by the Monte-Carlo technique. Also, the response function of the spectrometer was determined and folded with the calculated spectra to allow meaningful calculation-experiment comparisons even near the 14 MeV peak. Three-dimensional Monte-Carlo calculations were made with the MCNP code, using the EFF-3, FENDL-1 and JENDL-FF nuclear data libraries. The total leakage fluence is correctly predicted or slightly overestimated by all these evaluated data. However, its breakdown into energy bins shows considerable overestimations near 0.1 MeV for FENDL-1 and JENDL-FF and near 10 MeV for JENDL-FF, while EFF-3 on the whole reproduces the leakage spectra best. An analysis of existing differential experimental V(n,xn) data at 14 MeV incident energy agrees with these findings.

October 1998

CONTENTS

1. INTRODUCTION

Vanadium-based alloys are interesting, in several respects, as potential structural materials for fusion reactors. From the point of view of neutronics, one of the interesting features is a possible superior neutron economy, i.e., a favorable balance between absorption by (n,x) reactions and multiplication by (n,2n) reactions. According to calculations [1] using evaluated nuclear data for vanadium from the EFF-1 file, vanadium as structural material instead of steel may open the possibility of attaining a sufficient tritium breeding ratio in the blanket of a DEMO-like reactor without requiring a specific neutron multiplier such as beryllium or lead, resulting in considerable engineering and economic advantages. This is not possible in a blanket having steel structures.

The nuclear data that mainly determine the neutron economy are the integral cross sections of the absorption reactions and inelastic processes, including (n,2n), (n,np) etc., as well as the secondary energy and angular distributions of the neutrons emitted in such processes.

For a reliable assessment of vanadium in this respect, its evaluated nuclear data should be verified, 'benchmarked', by integral experiments, i.e., experiments on thick samples. A very suitable type of experiment consists in measuring the spectral leakage flux from spherical shells with a central neutron source, an experimental geometry that dates back to the pioneer times of neutron physics [2]. Compared with other geometries, the spherical symmetry (even if only near-perfect) greatly facilitates the measurements, since neutron fluence measurements at only one location outside the sphere suffice for determining completely the neutron leakage from the sphere. Also, neutron transport calculations are facilitated because the calculational problem is one-dimensional, i.e., the fluence from a given assembly depends only on the radial coordinate. With the advent of three-dimensional Monte Carlo transport codes such as MCNP [3] and suitable fast computers, the latter argument is less important now than it was in the past. In fact, the calculations presented in this report were all made in three-dimensional geometry with detailed modeling of the experiment, taking thereby into account the deviations from perfect spherical symmetry. Nevertheless, it remains a useful feature of this type of experiment that simplified 'scoping' calculations can be made with 1-dimensional transport codes.

In spherical shell transmission experiments with a given material and given source neutron spectrum, the only interesting parameter left for variation is the shell thickness. It is useful to investigate under otherwise identical conditions several thicknesses, ranging from about one to several mean free path lengths λ for 14 MeV neutrons. At 1 λ or less, the resulting leakage spectrum will differ from the spectrum of the bare neutron source essentially only by the effects of single collisions of 14 MeV neutrons, while at large thicknesses multiple collisions, including collisions at lower energies, will predominate. Observing specific features of the leakage spectrum as functions of thickness helps, therefore, to track down the responsible cross section quantities and energy ranges, and provides a broader basis for sensitivity studies.

In the experiment reported here, two spherical shells of 0.6 λ and 1.8 λ were used. The acquisition of a third, thicker shell was not possible due to limited funds. It is hoped that international collaboration will permit such an extension of the work in the near future. The present experiment was performed in collaboration between IPPE Obninsk and Forschungszentrum Karlsruhe. It appears to be the first integral

fast-neutron experiment ever performed on vanadium. Preliminary results (with conclusions slightly different from the present ones) were published elsewhere [4]. Similar experiments on vanadium are being performed at Japan Atomic Energy Research Institute, Tokai-mura, and at the Technical University of Dresden, Germany.

2. EXPERIMENT

2.1 Experimental arrangement

The work was performed at the pulsed neutron generator KG-0.3 in Obninsk using time-of-flight (TOF) neutron spectrometry. Fig. 1 gives an overview of the experimental arrangement.

Short bursts of 14 MeV neutrons were produced by the neutron generator using the T(d,n) reaction. The target assembly consisted of a conical aluminium tube of only 0.5 mm wall thickness. A solid titanium-tritium target on a copper radiator (11 mm diameter, 0.8 mm thick) was positioned at the end bottom of this tube in the geometrical center of the spherical shell. The deuteron beam was collimated by a diaphragm with an 8 mm hole.

For monitoring the neutron source strength, the α particles produced in the T(d,n)^{4}He reaction at a reaction angle of 175° were detected through a 1 mm diameter collimator by a silicon surface barrier (SSB) detector. The product of efficiency and solid angle of the SSB detector was measured with a calibrated ^{238}Pu source ($T_{1/2}$ = 86.4 a), which emits 5.5 MeV α particles. The Pu source took the position of the Ti-T target in this calibration measurement, thus keeping the source-detector geometry the same as in the neutron measurements.

The spectral neutron flux leaking from the outer surface of the sphere was detected by a fast scintillation detector at 6.8 m flight path. The detector was installed in a lead house behind a concrete wall at a reaction angle of 8°. A conical hole drilled through the wall acted as a collimator.

For measurements of the background (room scattered) neutron spectra, an iron shadow bar (1 m long by 18 cm or 26 cm in diameter) was placed between detector and sphere. To reach sufficient suppression of direct neutrons from the sphere, an additional 30 cm long borated polyethylene cylinder was mounted on the shadow bar. The position of the shadow bar was selected individually for each sphere to shadow only the shell, but not the shell holder.

2.2 Pulsed neutron generator KG-0.3

The neutron generator is a Cockcroft-Walton accelerator with an RF electromagnetic discharge ion source, RF deflection and a klystron bunching system [5]. The main specifications of the neutron generator are listed in Table 1.

Table 1. Main parameters of the neutron generator

Parameter	Value
Sort of accelerated particles	H or D
Maximum acceleration energy	280 keV
Energy of ions extracted from source	30 keV
Maximum ion current from source	1 mA
Ion pulse width	2.5 ns
Max. instantaneous current	0.6 mA
Beam spot diameter	5 mm
Period between pulses	$n \times 200$ ns, $n = 1 \div 15$
Mean beam current (at 1.25 MHz)	1 μA
Neutron yield	10^8 1/s

The chopping and bunching of the ion beam are carried out before acceleration. First the beam is deflected by a sinusoidal voltage of 10 MHz frequency or 100 ns period, so that 20 ns long beam pulses pass through a slit. Bunching of these ion pulses is carried out in a dual-gap buncher system at the same frequency. The buncher compresses the ion pulses down to 2 ns at the target location. To obtain the desired pulse period, a secondary beam deflecting system is used which lets only selected deuteron bursts pass through a diaphragm. The repetition period of the 50 ns-width secondary deflecting pulses can be set arbitrarily to $n \times 200$ ns (n = 1 - 15).

After high voltage acceleration the deuteron beam passes through an analyzing magnet, is focused by a magnetic quadrupole doublet and strikes the target. Usually, air cooled Ti-T targets on 11 mm dia. Cu backing are used in the neutronics experiments. About 50 cm before the target a pick-up electrode is placed inside the ion drift tube to derive the stop pulses for TOF measurements.

2.3 Spherical vanadium shells

Two spherical shells of vanadium of over 99% purity were manufactured at the Institute of Inorganic Materials. They are shown in Fig. 2. Their dimensions and masses are given in Table 2, where the unit λ denotes the mean free path of a 14-MeV neutron in vanadium. For accommodating the neutron source, i.e. the target assembly of the neutron generator, either sphere has a cylindrical radial hole, the bottom of which is hemispherical and concentric with the sphere surface. Sphere 1 is a single piece, while sphere 2 is composed of two hemispheres for reasons of both manufacture and handling in the experiments.

Table 2. Vanadium sphere dimensions and masses

Sphere	Sphere radius,	Hole radius,	Thickness		Mass
No.	cm	cm	cm	λ	kg
1	5.0	1.5	3.5	0.6	3
2	12.0	1.5	10.5	1.8	43

The density of either sphere was measured and found to agree well with the literature value of 6.09 g/cm^3. The material composition as specified by the manufacturer of the base material is given in Table 3.

Table 3. Specified impurities of vanadium metal

Element	Al	Fe	Si	C	N	H	O
Mass %	0.2	0.15	0.2	0.03	0.01	0.001	0.03

2.4 Detectors and electronics

The main neutron detector consisted of a paraterphenyl crystal of 5 cm diameter by 5 cm length, optically coupled to an FEU-143 photomultiplier. A block diagram of the electronic system is shown in Fig. 3. The TOF measurement is made in the usual 'inverse' variant, that is, using the detector signal as 'start' and the suitably delayed neutron source signal as 'stop'. This is chosen because only a small fraction of the neutron bursts results in detector pulses; the inverse TOF technique avoids useless starts of the time measuring device which otherwise would cause high dead time losses.

In the first series of measurements in 1996, the anode pulses were fed to a constant fraction discriminator and neutron-γ discriminator (FEI-BDK). The fast output of the BDK furnished the 'start' input for a time-to-digital-converter (TDC1, LeCroy 4201), which was gated by the 'neutron' output of the BDK (dashed line in Fig. 3). In the second measurement series in 1997, the anode pulses were split and fed to both a constant fraction discriminator (CFD, Canberra 2126) and a separate neutron-γ pulse shape discriminator (PSD, Canberra 2160A) to suppress γ ray signals. The fast CFD output, delayed by a delay generator (LD, Canberra 2055), furnished the start input to TDC1, which was gated by 'neutron' pulses from the PSD (solid lines in Fig. 3).

The neutron generator pulse mode was monitored by a 'time-of-flight monitor' consisting of a fast plastic scintillator (∅2 cm × 2 cm) and photomultiplier FEU-87. Its time reference pulses were derived by a constant fraction discriminator and fed to another time-to-digital converter (TDC2, FEI-VACP-5).

The signals from the SSB α particle detector, shaped and amplified by a preamplifier (PA) and linear Amplifier (AMP, Tesla NL2208), were fed to an analog-to-digital converter (ADC, FEI-ACP-9).

A cylindrical pick-up electrode detected the time of the deuteron burst going to the tritium target. Its fast signal, amplified by a preamplifier, triggered a fast discriminator (FD). The suitably delayed output pulse of this was used as 'stop' input to TDC1.

A Long Counter was used for monitoring the neutron yield. Its pulses were amplified (PA) and shaped by a discriminator (FD). To measure the dead time fraction, the pulses were then split and counted (1) continuously by one register of a multiple counter (MCC) and (2) by a gated monitor counter (MC). The gate pulse for MC was generated by a fan-in unit (OR) from the NAF signals of the slowest two of the converters.

The logic outputs from the discriminators and the 'look-at-me' (LAM) pulses from the converters were also registered by the multiple counter. The digital outputs of the converters as well as the MC and MCC contents were read via the CAMAC bus and stored in a 4 kB memory (M). This process was controlled by an Intelligent Controller

(IC, FEI-BAK01). After acquisition of a preset number of MC counts, all information was read out via a crate controller (POLON K-106A) to a computer (PC AT286).

The parameters of the electronic units were adjusted so as to obtain the best time resolution, low threshold and sufficient γ-ray suppression. The main detector had a time resolution of 3 ns, a threshold near 50 keV (see next section) and γ-ray suppression factor of about 3. The TOF monitor had a time resolution of less than 0.5 ns. The neutron burst repetition period and the conversion time range of TDC1 were selected at 3 μs to permit registration of neutrons with energies from 14 MeV down to 50 keV. The differential and integral linearities of the time-to-digital conversion over the full range were better than 0.5%.

2.5 Neutron detector efficiency

Neutron detector efficiency as a function of neutron energy is one of the most important parameters. Its accuracy directly affects the accuracy of final results. This is why the efficiency was measured several times by two methods. Additionally, several Monte-Carlo calculations were made to estimate the influence of different effects (see chapter 3).

The detector efficiency was experimentally determined by measuring spectra of neutrons from the spontaneous fission of ^{252}Cf, which is known in the range 0.1 MeV to 10 MeV with 3% accuracy [6]. The ^{252}Cf neutron source is simultaneously a fission chamber, so that the number of fissions as well as the time moment of every disintegration (about 5×10^5 per second) could be obtained by registration of the chamber pulses. A discriminator threshold suppressed low amplitude pulses originating from α particles. The output signal of the discriminator was used as the stop pulse for the time-of-flight measurement and for counting the total of fission fragments N_{FF}. After background subtraction and conversion of the TOF spectrum into the energy spectrum $N(E)$, the detector efficiency was calculated according to

$$e(E) = \frac{N(E)}{nc(E)N_{FF}\Omega_D} \tag{1}$$

with

$\nu = 3.7661$	number of prompt neutrons per fission of ^{252}Cf (Ref. [7])
$\chi(E)$	energy spectrum of ^{252}Cf neutrons, normalized to $\int_0^\infty c(E)dE = 1$ (Ref. [6])
$\Omega_D = \pi (r/L)^2$	detector solid angle
r	detector radius
L	flight path between Cf chamber and detector.

Since in the high energy range (> 6 - 10 MeV) the number of fission neutrons becomes too small, another method was used for efficiency calibration there. At 14 MeV, the detector efficiency was determined by simultaneous measurements of both the neutron (Y_n) and associated α particle (Y_α) yields from the T+d reaction:

$$e(14\ \text{MeV}) = \frac{Y_n R_n(8^\circ) e_a \Omega_a R_a(175^\circ)}{Y_a \Omega_D} \qquad (2)$$

with

$R_n(8°) = 1.05$ anisotropy coefficient for neutrons emitted from the thick tritium target at 8° (Ref.[8])

$R_\alpha(175^\circ) = 1.253$ anisotropy coefficient for α particles emitted at 175° (Ref.[8])

$e_a W_a$ product of efficiency and solid angle for the α particle detector.

The latter quantity was measured using a ^{238}Pu α particle source with known activity A_{Pu}:

$$e_a \Omega_a = 4p \frac{Y_{a,Pu}}{A_{Pu}} \qquad (3)$$

The detector efficiency measured by these techniques is shown in Fig. 4. It is seen that the detector threshold is about 40-50 keV for the experiment of 1996 (constant fraction discriminator FEI-BDK) and 60-70 keV in the experiment of 1997 (CFD Canberra 2126), and the efficiency in the range 0.2-4 MeV had approximately constant values of about 0.55 and 0.43 respectively. The latter difference may be due, e.g., to different γ ray suppression factors in the two circuits.

2.6 Measuring procedure and data processing

For every shell the TOF spectra were measured many times with and without shadow bar (background and foreground) in order to average out possible fluctuations of the spectrometer parameters. The spectrometer parameters themselves were measured periodically throughout the experiment duration.

The accumulated single experimental spectra were checked from the point of view of consistency, and 'bad' spectra were rejected. The remaining spectra were shifted along the time axis to remove time drifts. For this procedure the position of the centroid of the 14 MeV peak was calculated and verified. Finally, summed foreground and background TOF spectra were obtained. After normalization of the background spectrum to the same number of Long Counter counts as the foreground spectrum and subtraction from the foreground spectrum, the resulting TOF distribution was converted to an energy spectrum *N(E)*. The finally interesting quantity is the differential fluence of leakage neutrons, integrated over the full sphere (4π sr) and normalized to 1 source neutron. This will be denoted leakage spectrum, *L(E)*, in this paper. It was calculated from $N(E)$ according to

$$L(E) = 4p \frac{N(E)}{e(E)\Omega_D N_n} \qquad (4)$$

where N_n is the total number of source neutrons. N_n was calculated from the total

number of α particles N_α measured simultaneously with the leakage spectrum:

$$N_n = \frac{N_a R_a (175^\circ)}{e_a \Omega_a} \tag{5}$$

2.7 Uncertainty of experimental data

The estimated uncertainties of the experimental data and their main components are listed in Table 4. Their dependence on leakage neutron energy in case of shell #1 is shown in Fig. 5.

The statistical uncertainty mostly has small values (about 4%). Only at energies close to the detector threshold it reaches dozens of percents.

Table 4. Uncertainties of experimental data

#	Component	Value	Energy dependence
1	Statistics	2 - 50%	Yes
2	Stability of equipment	3 - 5%	Yes
3	^{252}Cf fission spectrum	1 - 3%	Yes
4	^{238}Pu α-intensity	~ 2%	No
5	Correction calculations:		
5.1	Cf-chamber scattering	1%	No
5.2	TOF-to-energy conversion	2%	No
	Total	5 - 50%	Yes

During the experiments the main spectrometer parameters (detector efficiency, absolute normalization factor etc.) were measured several times. Thus the stability of the spectrometer, component #2 in the table, could be estimated by calculating the mean square deviation of individual runs.

In the experiment two radioactive reference sources were used: ^{252}Cf for neutron detector calibration and ^{238}Pu for α detector calibration. They have specific uncertainties also shown in Table 4.

The uncertainties of corrections for Cf-chamber scattering and time-of-flight conversion to energy, calculated with MCNP, were estimated at about 1-2%.

We denote the quadratic sum of components 2-5 in Table 4 as systematic uncertainty. Quadratic summation of the statistical and systematic uncertainties yields the total uncertainty of the experimental data.

2.8 D(d,n) neutron contribution

It is well known that during irradiation of a solid tritium target, part of the beam deuterons are implanted in the target and create an additional source of neutrons from the D(d,n) reaction with energies around 2.5 MeV. Such neutrons are seen in the spectrum measured with the bare target assembly, as shown in Fig. 6. To estimate the contribution of these neutrons we calculated the area under the D(d,n) peak in the source neutron energy spectra measured several times during the experiment. The

ratio of neutron yields from D(d,n) and T(d,n) reactions is shown in Fig. 7 as a function of deuteron beam irradiation time, the mean current being 0.5 μA. It is seen that this ratio continuously increased and reached the value of 0.3% at the end of the experiment (for comparison let us remind that the total contribution of target assembly scattered neutrons is 3%). To decrease the effect of D(d,n) neutrons the TiT target was rotated around its axis, which resulted in irradiation of a 'fresh' zone of the target, since the deuteron beam was apparently slightly shifted from the target center.

3. MONTE CARLO SIMULATION OF EXPERIMENTAL DETAILS

Three-dimensional Monte Carlo simulations of details of the experiment have been made with the MCNP-4A code [3] to obtain corrections for certain effects that are usually neglected. The nuclear data for these calculations were taken mainly from the Fusion Evaluated Nuclear Data Library FENDL-1 [9]. Similar calculations were made earlier for the case of iron shells [10, 11].

3.1 Time-of-flight measuring technique in case of bulk samples

The time-of-flight method presupposes a strict relation between the neutron energy E, the sample-detector distance L and the flight time t:

$$E = mc^2 (1/\sqrt{1-(L/ct)^2} - 1) \approx (72.3 \cdot L[\,\mathrm{m}\,]/t[\,\mathrm{ns}\,])^2 \qquad (6)$$

where: m - neutron mass,
c - light velocity in vacuum.

This equation is fulfilled if the dimensions of source, sample and detector can be neglected in comparison with the detector-sample distance. However, in benchmark experiments of the spherical-shell transmission type, the size of the sample assembly in general is not negligible. In the present experiment, the radius of sphere 2 is 1.8% of the sphere-detector distance, and by multiple scattering a neutron may travel within the sphere a path several times longer than the radius.

The consequences of this experimental geometry can be evaluated because the MCNP code calculates both the energy and the time of arrival of a neutron at the detector. With proper, detailed modeling, the calculations take into account the real geometry of the experiment and the real travel time that the neutron spends on its way from the source via the sample sphere to the detector. The time distribution of the neutrons arriving at the detector position, referred to the start of the neutron from the source as zero time, can then be converted to an energy spectrum using the above equation. This procedure is a simulation of the time-of-flight experiment together with its data reduction procedure. The leakage spectrum $L(E(t))$ obtained in this way ('time-dependent Monte-Carlo technique') can be compared with the energy distribution $L(E)$ of the neutrons calculated directly by the MCNP code, without considering any time relationship ('time-independent Monte-Carlo technique'). This results in a correction function $C_t(E)=L(E)/L(E(t))$, which should be multiplied to an experimental spectrum before comparing it with a Monte-Carlo spectrum calculated in the time-independent way. The energy dependence of $C_t(E)$ is shown in Fig. 8 for both of the vanadium shells. It is seen that this correction for shell 2 will increase the measured leak-

age spectrum in the energy range 1 - 10 MeV by 2%, but decrease it at energies below 1 MeV, while it has practically no effect for shell 1.

Time delays of neutrons, due to longer distances covered within the sphere by scattering, result in a further effect, an apparent shift of resonances to lower energies in the spectrum obtained by the time-dependent technique. In Fig. 9, which shows $L(E)$ and $L_t(E(t))$ separately for shell 2, such a shift is clearly noticeable in the energy range below 1 MeV. Similar shifts were originally seen in our experimental data on iron spheres [10]. This led us to perform the above calculational investigation.

3.2 Corrections for non-spherical effects

Many transport codes (e.g., ANISN, ONEDANT, ANTRA-1 etc.) use the one-dimensional (spherical) approximation. Such calculations would be immediately comparable only with the results of an ideal benchmark experiment which is spherically symmetric in every respect. The real experiment deviates from perfect spherical symmetry because of:

1. the beam hole (channel) in the shell,
2. the non-spherical matter distribution of the target assembly,
3. the dependence of both source neutron energy and differential source strength (i.e., yield per element of solid angle) on the reaction angle.

The experimental data have to be corrected for these effects before they can be compared with 1-dimensional code results.

The influence of the hole has been estimated by comparison of leakage spectra calculated for shells without ($L(E)$) and with ($L_h(E)$) the hole. In the calculation the detector was placed at distance 6.8 m and angle 8^o relative to the deuteron beam (see Fig. 1). The corresponding correction function $C_h(E) = L(E)/L_h(E)$ is shown in Fig. 10 for two vanadium shells. It is seen that the correction anticorrelates with the relative hole volume and has a maximum value of 10% for the smaller shell 1.

The non-spherical distribution of matter other than the sample shell, i.e. the target assembly, leads to spectral modifications of the neutrons entering the sample and to an angle-dependent flux attenuation of the uncollided (14-MeV) neutrons. For the target assembly described above, the calculated angular distribution of 14-MeV neutrons is shown by the dashed curve in Fig. 11. The attenuation is strongest (7-10%) at angles close to 90^o and 150^o, where the material thickness is largest. Nevertheless the total (4π sr integrated) attenuation is relatively small, 2.5%.

The flux of lower-energy neutrons produced by inelastic neutron interactions in the target assembly is much less dependent on angle, because these processes distribute their product neutrons through the total 4π sr solid angle. It is a reasonable approximation to assume the part below the 14-MeV peak in the spectrum of neutrons entering the sample shell to be isotropic.

The T(d,n)^{4}He reaction at deuteron energies below 300 keV is very accurately isotropic in the center-of-mass coordinate frame [12]. The anisotropies of both source neutron energy and yield in the laboratory frame are, therefore, purely due to the kinematic coordinate transformation, so that they can be calculated. The resulting angular dependencies [13] of these quantities for our case are shown by the solid curves in Fig. 11. The yield anisotropy amounts to about ±6%.

3.3 Correction to neutron detector efficiency calibration

The Cf-252 fission chamber consists of thin and light materials. Nevertheless, a distortion of its spectrum due to neutron scattering by the chamber materials is still possible. To estimate this effect, the neutron interaction with the Cf chamber was simulated by Monte-Carlo calculations [10, 11]. In this case nuclear data from the EFF-1 library were used. Fig. 12 shows the ratios of several spectra calculated for the detector location to the pure Cf-252 emission spectrum taken from Ref. [6]. The influences of different factors were analyzed.

The solid line shows the distortions of the Cf spectrum resulting only from scattering of neutrons on the chamber materials. The long-dashed line shows the influence of the air (the distance between Cf chamber and detector is about 5 m), which results in an attenuation of the flux above 3 MeV and an increase below 3 MeV. The short-dashed line shows the scattering of neutrons on the walls of a 1m long concrete collimator (see Fig. 1), which increases the effective solid angle and softens the spectrum by scattering on the collimator materials.

During efficiency measurements, the detector views not only the TiT-target assembly but also the deuteron beam tube including massive parts such as quadrupole lenses and flanges (Fig. 1). Simulation of these elements shows that the contribution from beam tube scattering at the detector location is negligible (dotted curve).

All or some of these effects should be taken into account if the detector efficiency is theoretically calculated or measured in conditions different from those where the neutron leakage spectra are measured. In our case, there is only one factor (influence of chamber material) which we have to take into account, since the influence of air and collimator is the same in efficiency and neutron leakage spectra measurements. It is seen that neutron scattering on the chamber materials changes the flux by up to 4% in the low energy part. This correction was applied in processing our experimental data.

4. SPECTROMETER RESPONSE FUNCTION

4.1 General

The result of a fast neutron spectrum measurement depends not only on the true energy distribution of the neutrons and on the spectrometer efficiency, but also on the finite energy resolution of the spectrometer, which in general varies with energy. The spectrometer can be completely characterized by its response function or response matrix $P(E,k)$, which is the probability that a neutron of energy E will produce a count in channel k of the spectrum. The efficiency $e(E)$ discussed in chapter 2 is the sum of $P(E,k)$ over all k. The measured spectrum is the folding (convolution) of the true neutron energy distribution with $P(E,k)$.

A spectrum obtained from a neutron transport calculation is a pure neutron energy distribution. For its meaningful comparison with a measured spectrum, it should first be folded with the response function; otherwise, discrepancies will appear at peaks and steep slopes in the spectrum, as seen, e.g., in Ref [4]. Therefore, the response function $P(E,k)$ needs to be determined. This is possible experimentally for energies E for which monoenergetic neutrons are available, in the present case, at 14 MeV.

4.2 Response function at 14 MeV

The experimental and Monte-Carlo calculated energy spectra of the bare neutron source are shown in Fig. 6 for the detector angle 8^o. Besides the '14-MeV' peak there is a broad low energy (0.2 - 5 MeV) distribution, which is caused by non-elastic scattering of neutrons in the target assembly. Discrepancies between the experimental and calculated spectra may be explained by underestimation of direct inelastic scattering in the evaluated nuclear data file used (FENDL-1) and by neutron scattering in the lead shield of the detector. As mentioned above, the low energy part of the source spectrum is assumed to be independent of emission angle, whereas the mean energy of the '14-MeV' peak is somewhat angle dependent as shown in Fig. 11.

The energy spectrum of the bare neutron source was used to obtain experimentally the spectrometer response function for 14 MeV neutrons. For this purpose, the low energy tail of scattered neutrons had to be removed. The tail was assumed to result from inelastic scattering of 14 MeV neutrons on copper, the predominant structural material near the Ti-T layer. The energy spectrum of neutrons from the Cu(n,xn) reaction was taken from the evaluation of Ref. [14]. This continuum is shown in Fig. 6 by a dotted line. By subtracting it from the measured source neutron spectrum, the dashed line in Fig. 6, the response curve for pure 14 MeV neutrons, was obtained.

4.3 Response function at lower energies

For energies *E* below the 14 MeV peak, sources of monoenergetic neutrons were not available. The corresponding response curves, therefore, had to be determined by calculation. The integral of each curve *P(E,k)* for a given *E* is the efficiency *e(E)*, determined as described in chapter 2. For the shape of the curves, reasonable assumptions had to be made. From 14 to 10 MeV the shape of the 14 MeV response curve was used by proportional scaling on the energy axis. At energies below 10 MeV, the shape was assumed to be Gaussian. The relative width *DE/E* of the Gaussian was calculated from the electronic time resolution *Dt/t* and the flight path uncertainty *DL/L*. This is less accurate than a response curve measured with a clean monoenergetic neutron source, but it is fully sufficient for the present purpose, because in the flat lower-energy continuum of the spectra the effects of the energy resolution are small. In fact, the folding of calculated neutron spectra with the response function resulted in important modifications only in the 10 - 12 MeV region. This is seen in Fig. 13, where the effect of the folding for a FENDL-1 calculation is shown for both spheres.

5. EXPERIMENTAL RESULTS AND COMPARISON WITH TRANSPORT CALCULATIONS

5.1 Consistency of 1996 and 1997 results

As described above, the neutron leakage spectra from the vanadium shells were measured twice, in 1996 and in 1997, with slightly different electronics. The results of the two experiments are compared in Fig. 14 (energy spectra) and in Table 5 (energy bin integrals). The uncertainties listed in Table 5 are only statistical. The differences between the 1996 and 1997 results are in the range of 1-7%, not exceeding the estimated total uncertainties.

Table 5. Comparison of leakage fluences from vanadium shells 1 and 2 measured in 1996 and 1997 (ratios with statistical uncertainties)

Energy Range, MeV	Shell 1 Ratio '1997/1996'	Shell 2 Ratio '1997/1996'
0.05 - 0.09	1.02 ± 0.49	0.98 ± 0.26
0.9 - 0.2	0.95 ± 0.04	1.08 ± 0.03
0.2 - 0.4	0.94 ± 0.02	0.99 ± 0.01
0.4 - 0.8	0.98 ± 0.01	1.02 ± 0.01
0.8 - 1.40	0.98 ± 0.01	1.01 ± 0.01
1.40 - 2.50	0.99 ± 0.01	1.02 ± 0.01
2.50 - 4.00	0.99 ± 0.01	1.01 ± 0.01
4.00 - 6.50	1.01 ± 0.01	1.02 ± 0.01
6.50 - 10.50	1.03 ± 0.02	1.04 ± 0.02
> 10.50	0.93 ± 0.05	0.97 ± 0.06
Total (>0.05)	0.95 ± 0.04	1.00 ± 0.02

5.2 Comparison with calculated leakage spectra

The final neutron leakage spectrum for each vanadium shell has been obtained by averaging the experimental results of the two years. These spectra and corresponding energy bin integrals are presented in Figs. 15 - 16 and Tables 6 - 7 respectively, together with the results of Monte Carlo transport calculations.

Three-dimensional Monte-Carlo transport calculations were made with the MCNP code, version 4A [3], and evaluated nuclear data for V-51 (which is 99.75% of natural vanadium) from

- the Fusion Evaluated Nuclear Data Library, FENDL-1 [9] (the reference file for the International Thermonuclear Experimental Reactor project, ITER),
- the European Fusion File EFF-3,
- the Japanese Evaluated Nuclear Data Library - Fusion File, JENDL-FF.

Each sphere with its hole and material composition was precisely modeled. As an improvement over the preliminary calculations presented earlier [4], the neutron source was modeled with the actual dimension of the deuteron beam spot on the target, i.e. a

5 mm diameter disc, and with the anisotropic energy and yield distributions of T(d,n) neutrons as discussed earlier. Besides 14 MeV neutrons the low energy continuum resulting from interaction of 14 MeV neutrons with target materials was also taken into account. The MCNP 'ring detector' was placed at the same distance from the sphere center (6.8 m) and angle relative to the beam axis (8^o) as in the experiment.

The calculated leakage spectra were folded with the detector response function as discussed above. The folded differential energy spectra calculated from all evaluated data files are included in Figs. 15 and 16 (top parts). Ratios *C/E* of calculated to experimental energy bin integrals are plotted in the bottom parts of the same figures. The *C/E* graphs clearly show that, for either sphere,

- below 1 MeV, FENDL-1 and JENDL-FF overestimate the neutron leakage considerably, whereas EFF-3 agrees better with measurement,
- in the medium energy range (1.4 – 6 MeV), EFF-3 overestimates the leakage somewhat more than the other files do,
- in the 7 – 12 MeV range JENDL-FF again overestimates considerably,
- the only significant underestimation is found near 1 MeV with FENDL-1.

Table 6. Measured neutron leakage fluences (averaged over 1996 and 1997 experiments) and calculation-over-experiment ratios *C/E* for V sphere #1.

Energy range, MeV	Experiment	*C/E* EFF-3	*C/E* FENDL-1	*C/E* JENDL-FF
0.05 - 0.09	(4.47 ± 1.00) E-03	0.98± 0.22	1.13 ± 0.25	0.85 ± 0.19
0.09 - 0.2	(1.43 ± 0.19) E-02	1.09 ± 0.14	1.59 ± 0.21	1.33 ± 0.17
0.2 - 0.4	(2.70 ± 0.12) E-02	1.01 ± 0.05	1.35 ± 0.06	1.41 ± 0.06
0.4 - 0.8	(5.54 ± 0.23) E-02	1.02 ± 0.05	1.08 ± 0.05	1.30 ± 0.06
0.8 - 1.4	(7.17 ± 0.29) E-02	1.08 ± 0.04	0.95 ± 0.04	1.06 ± 0.04
1.4 - 2.5	(7.01 ± 0.32) E-02	1.22 ± 0.05	1.01 ± 0.05	1.11 ± 0.05
2.5 - 4.0	(4.12 ± 0.12) E-02	1.21 ± 0.05	1.15 ± 0.05	1.05 ± 0.04
4.0 - 6.5	(2.82 ± 0.16) E-02	1.07 ± 0.06	1.19 ± 0.07	1.12 ± 0.06
6.5 – 10.5	(2.11 ± 0.12) E-02	1.17 ± 0.04	1.27 ± 0.05	1.51 ± 0.06
> 10.5	(7.00 ± 0.07) E-01	1.08 ± 0.11	1.07 ± 0.11	1.08 ± 0.11
Total (> 0.05)	(1.03 ± 0.06) E+00	1.09 ± 0.09	1.09 ± 0.09	1.11 ± 0.09

Table 7. Measured neutron leakage fluences (averaged over 1996 and 1997 experiments) and calculation-over-experiment ratios *C/E* for V sphere #2.

Energy range, MeV	Experiment	*C/E* EFF-3	*C/E* FENDL-1	*C/E* JENDL-FF
0.05 - 0.09	(2.04 ± 0.31) E-02	1.02 ± 0.28	1.19 ± 0.35	1.01 ± 0.30
0.09 - 0.2	(6.48 ± 0.86) E-02	1.18 ± 0.15	1.50 ± 0.20	1.49 ± 0.20
0.2 - 0.4	(9.30 ± 0.43) E-02	0.98 ± 0.04	1.14 ± 0.05	1.28 ± 0.06
0.4 - 0.8	(1.75 ± 0. 08) E-01	0.95 ± 0.04	0.95 ± 0.04	1.13 ± 0.05
0.8 - 1.4	(1.77 ± 0.07) E-01	1.03 ± 0.04	0.92 ± 0.04	0.98 ± 0.04
1.4 - 2.5	(1.25 ± 0.06) E-01	1.19 ± 0.05	1.01 ± 0.05	1.03 ± 0.04
2.5 - 4.0	(6.10 ± 0.26) E-02	1.15 ± 0.05	1.11 ± 0.05	0.97 ± 0.04

4.0 - 6.5	(3.64 ± 0.20) E-02	1.09 ± 0.06	1.20 ± 0.07	1.17 ± 0.06
6.5 – 10.5	(2.47 ± 0.14) E-02	1.02 ±0.05	1.07 ± 0.05	1.41 ± 0.07
> 10.5	(3.67 ± 0.37) E-01	1.05 ± 0.11	1.04 ± 0.10	1.04 ± 0.10
Total (> 0.05)	(1.14 ± 0.07) E+00	1.06 ± 0.07	1.05 ± 0.07	1.11 ± 0.07

5.3 Total leakage neutron multiplication

The total effective leakage neutron multiplication (obtained by integration of leakage spectra from 50 keV to 14 MeV) is given in the bottom lines of Tables 6 and 7. It plausibly increases with wall thickness: 1.03 for shell 1 and 1.14 for shell 2. Our preliminary experimental results [4], based on the 1996 measurements, differed from these by +3% for shell 1 and -3% for shell 2, i.e. within experimental uncertainty. Both the EFF-3 and FENDL-1 libraries overestimate the total multiplication by about one experimental uncertainty, while the overestimation by JENDL-FF is more pronounced.

6. DISCUSSION

6.1 Energy bin *C/E* ratios

At 7 - 10 MeV, the leakage from shell 1 is overestimated by all evaluated data files, while for shell 2 the FENDL-1 and EFF-3 results are close to experiment. This can be explained by an underestimation of the Cu(n,xn) continuum in the source spectrum, leading to overestimation of the low energy tail of the 14-MeV response curve (see section 4.2). For the thicker shell 2, the relative size of the 14 MeV peak and thus the influence of the response curve is smaller. This means that the leakage overestimation at 7 - 10 MeV with FENDL-1 and EFF-3 is mainly caused by the imperfection of our 14-MeV response curve. The larger overestimation by JENDL-FF in this energy bin, however, is observed with either shell thickness and must be due to that data evaluation.

The slight underestimation of the leakage fluence near 1 MeV by the FENDL-1 data for both of the shell thicknesses might indicate low values of the V(n,2n) and/or (n,np) cross sections, since these processes populate specifically the 'evaporation peak' region around that energy.

At material thicknesses not much larger than the mean free path, the transport of 14 MeV neutrons is mainly determined by elastic and inelastic scattering at this incident energy. Therefore, it is useful to complement the benchmark results by analyses of the corresponding 14 MeV microscopic data. In case of vanadium, the (n,n') and (n,2n) channels are the predominant neutron production reactions.

Double differential neutron emission cross sections for vanadium have been measured by several groups [15-18]. Their results for the angle-integrated $d\,s/dE_{out}$ cross section or secondary energy distribution (SED) are shown in Fig. 17 (except Ref.[18] which contradicts the others very seriously). For the sake of convenience, the top half of the figure shows the low energy part of the secondary neutron spectrum on a logarithmic energy scale, the bottom half the high energy part on a linear energy scale. The evaluated SED for 14 MeV neutrons derived from the FENDL-1, EFF-3 and JENDL-FF libraries are also shown in the figure. They were obtained by calculating the spectrum outside a thin vanadium spherical shell (wall thickness <1 mm) by the

MCNP-4A code.

In the low energy part (0.1 to 1 MeV) of the secondary spectrum, EFF-3 has the smallest cross sections in comparison with the other two libraries. It is seen that experimental data for the SED do not exist in this energy range because of the relatively high thresholds of the detectors used. So the evaluated cross sections could not be verified against microscopic data.

In our integral benchmark experiment the detector threshold was much lower and we succeeded in the measurement of neutron leakage in the energy range below 1 MeV, where the SED predicted by the different libraries differ much. The results obtained for both of the vanadium spheres show definitely that EFF-3, which predicts less leakage neutrons of these energies, agrees best with experiment.

In the middle (3 - 7 MeV) and especially in the high (>7 MeV) energy range, as seen in Fig. 17, the disagreement between the experimental microscopic data of the different groups increases. This results in a wide corridor in which the selection of the correct energy dependence of the SED becomes problematic. Correspondingly, a large scatter of the predictions of the different libraries is clearly visible in the high energy part of the leakage spectra from vanadium shells; e.g., the high *C/E* found with JENDL-FF around 10 MeV may reflect the high experimental cross section data of Ref.[15] seen in Fig. 17. The analysis of the present integral benchmark experiment (see 5.2) has shown, however, that EFF-3 is closer to reality than the other libraries also in the energy range 4 - 10 MeV.

This example confirms that integral benchmark experiments are suitable to give additional and even decisive information for the verification of evaluated data files.

6.2 Total leakage neutron multiplication

The overestimation of the total leakage fluence from either sphere is not far beyond experimental uncertainty, in contrast to some of the energy bin results. This is not surprising, since overestimations and underestimations in different bins compensate each other in the sum. Similar experiences were made earlier in benchmarking evaluated data for beryllium [19,20]. They demonstrate again that benchmarking evaluated nuclear data by spherical shell transmission experiments requires measurements of the spectral, and not only the total, leakage fluence.

ACKNOWLEDGEMENTS

We thank Dr. U. Fischer for many useful hints and advice.
The IPPE authors are grateful to the International Atomic Energy Agency for supporting this work under Contract No. 9268.

REFERENCES

1. U. Fischer, unpublished, 1994

2. H.A. Bethe, J.R. Beyster and R.E. Carter,
J. Nucl. En., 1956, v.3, p. 207 and 273; 1957, v.4 , p. 3 and 147

3. J. F. Briesmeister (ed.), Report LA-12625-M, 1993

4. U. von Möllendorff, B. V. Devkin et al., in: Fusion Technology 1996
(C. Varandas and F. Serra, eds.), Elsevier, Amsterdam, 1997, p. 1575

5. A.B. Anufrienko et al., Voprocy Atomnoi Nauki i Techniki,
Seriya: Reaktorostroenie, 1977, v. 5 (19), p. 11

6. W. Mannhart, in: report IAEA-TECDOC-410, Vienna, 1987, p. 158

7. Nuclear Data Standards for Nuclear Measurements,
report INDC(SEC)-101, Vienna, 1992

8. I. Ruby, R. B. Crawford, Nucl. Inst. Meth., 1963, v. 24, p. 413

9. S. Ganesan, P. K. McLaughlin, report IAEA-NDS-128, Vienna, 1994

10. B. V. Devkin, U. Fischer, F. Kappler et al., report FZKA 5862, Karlsruhe, 1996

11. B. V. Devkin, U. Fischer, F. Kappler et al., Voprocy Atomn. Nauki I
Techn., Seriya Yadernye Konstanty, Obninsk, 1997, v. 1-2, p. 38

12. H. Liskien and A. Paulsen, Nucl. Data Tables, 1973, v. 11, p. 569

13. J. Csikai et al., in: report IAEA-TECDOC-410, Vienna, 1987, p. 296

14. A. Pavlik and H. Vonach, Physik Daten, Fachinformationszentrum, Karlsruhe,
1988, v. 13, No 4

15. M. Baba, M. Ishikawa, report NETU-50, Tohoku University, 1988

16. W. Hermsdorf, A. Meister et al., Kernenergie, 1974, v. 17, p. 176

17. A. Takahashi, E. Ichimura et al., OKTAVIAN Report A-87-03, Osaka, 1987

18. S. C. Mathur, P. S. Buchanan et al., Phys. Rev., 1969, v. 186, p. 1038

19. U. von Möllendorff, A.V. Alevra, H. Giese et al., Fusion Eng. Des., 1995,
v. 28, p. 737

20. U. Fischer and U. von Möllendoff, Fusion Techn. 1993, v. 24, p. 229

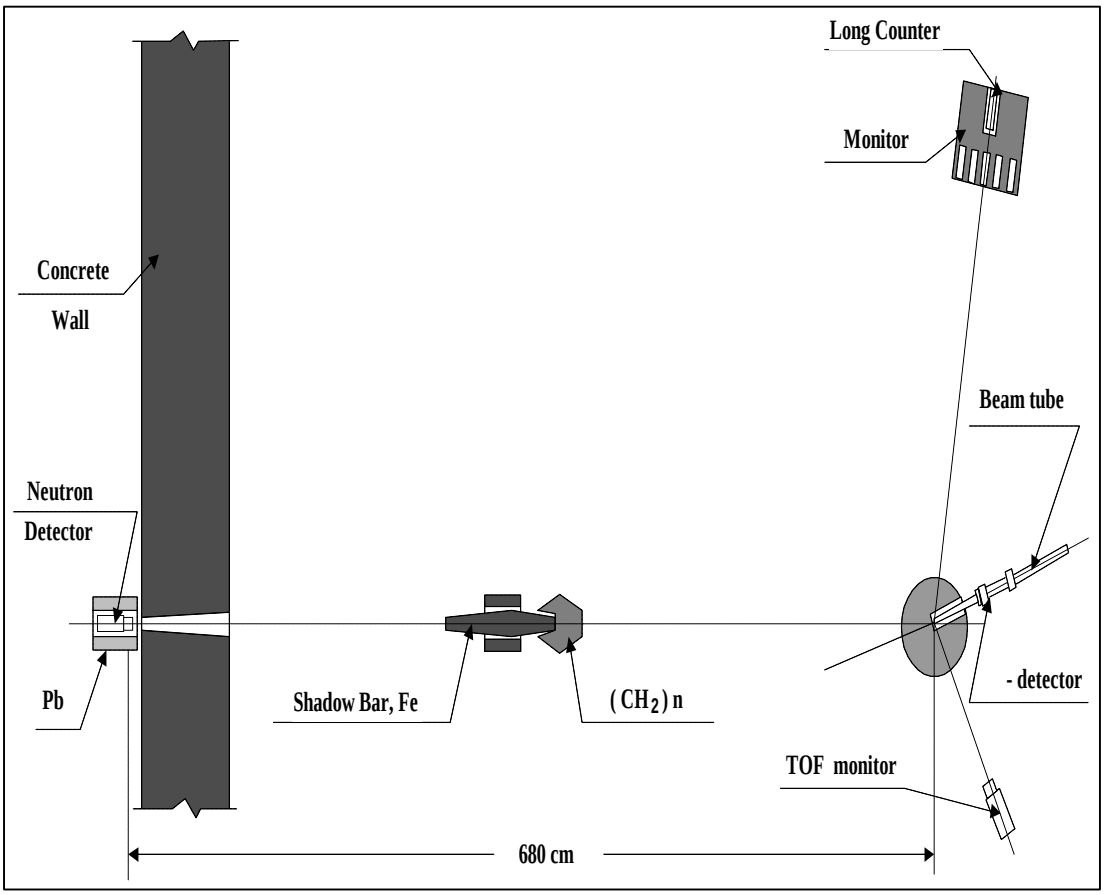

Fig. 1. Lay-out of experiment for measuring the neutron leakage spectra from vanadium spheres.

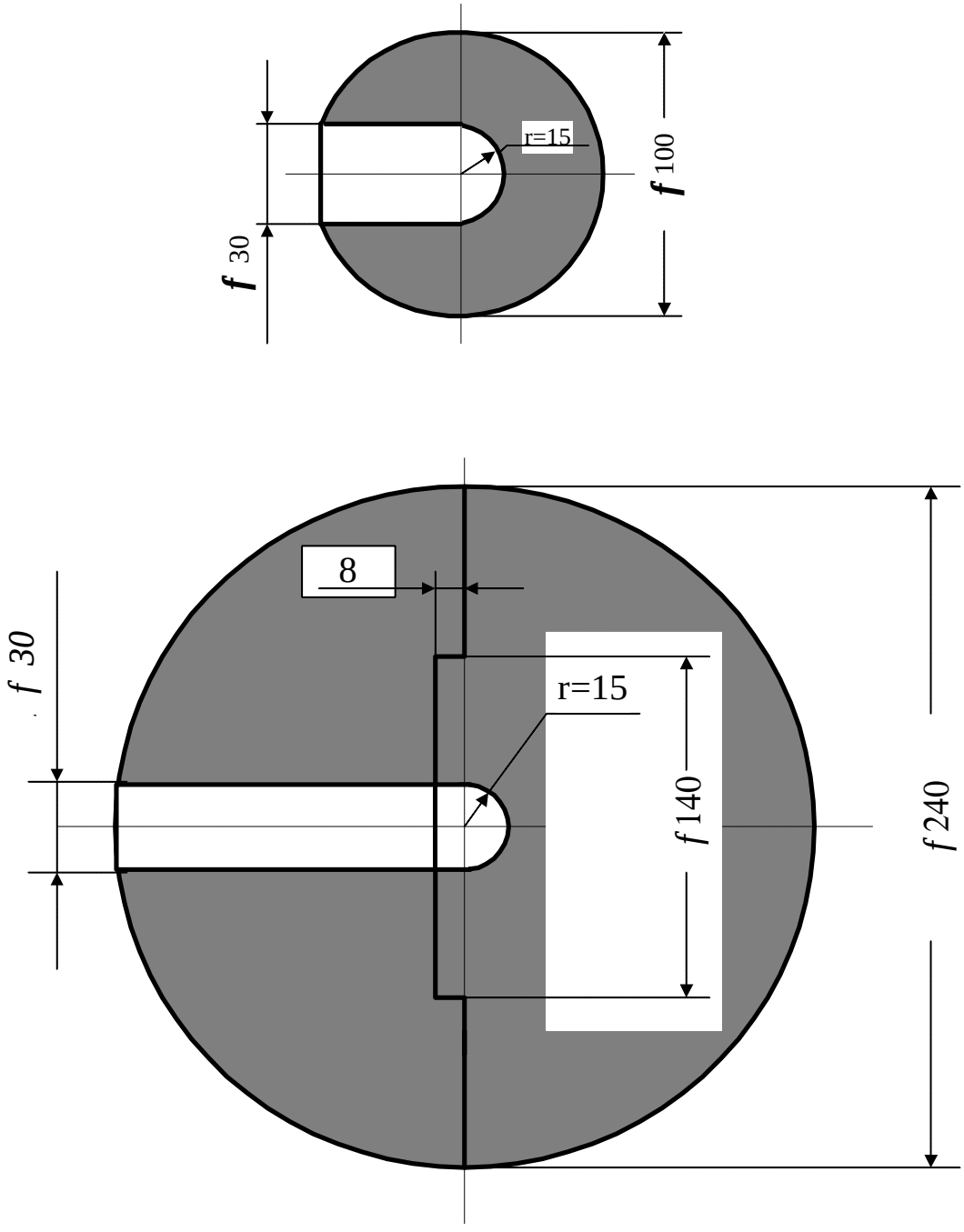

Fig. 2. Configuration of vanadium spheres # 1 (upper) and # 2 (down).

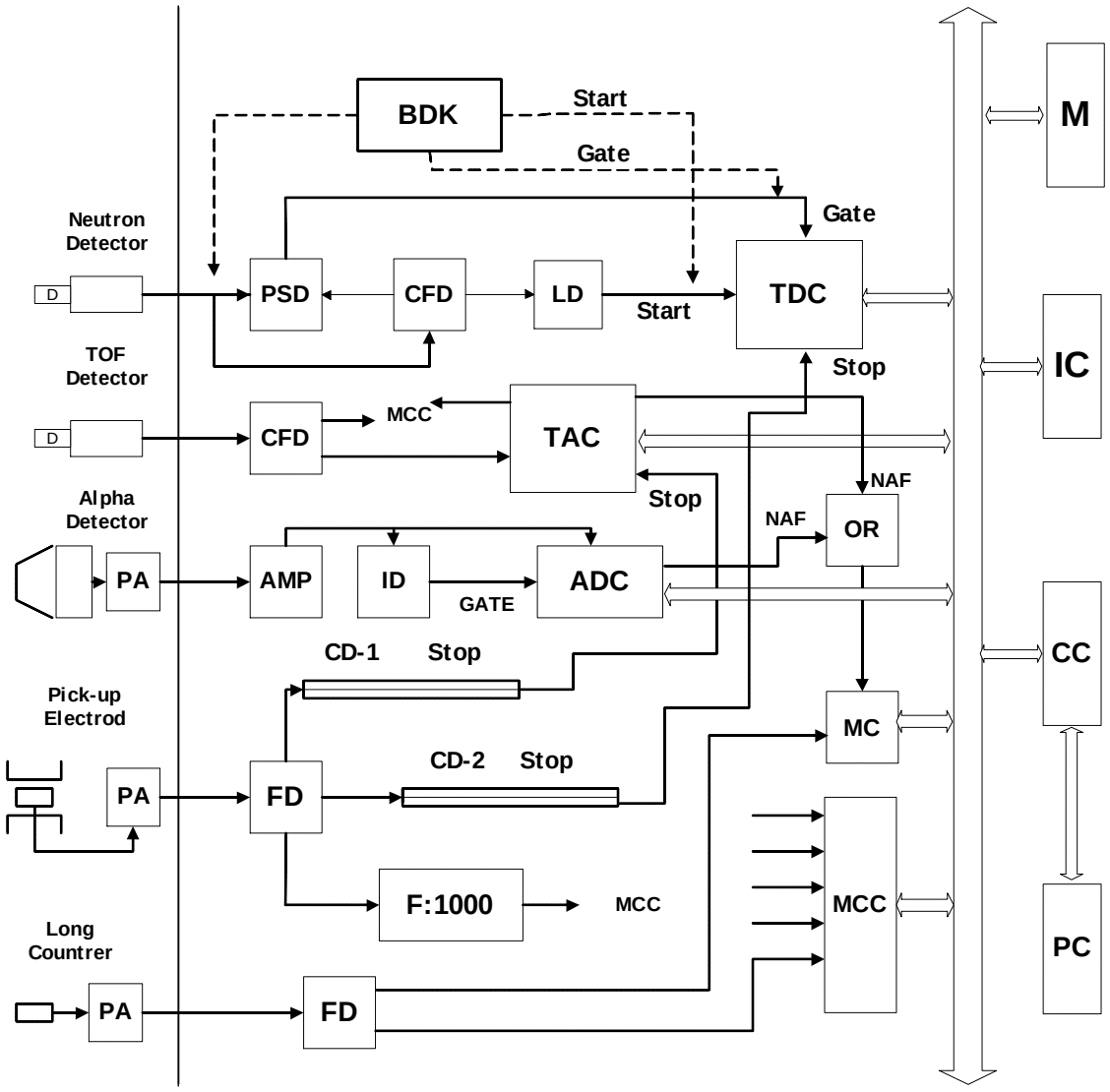

Fig. 3. Block scheme of electronic circuit (see section 2.4 for description).

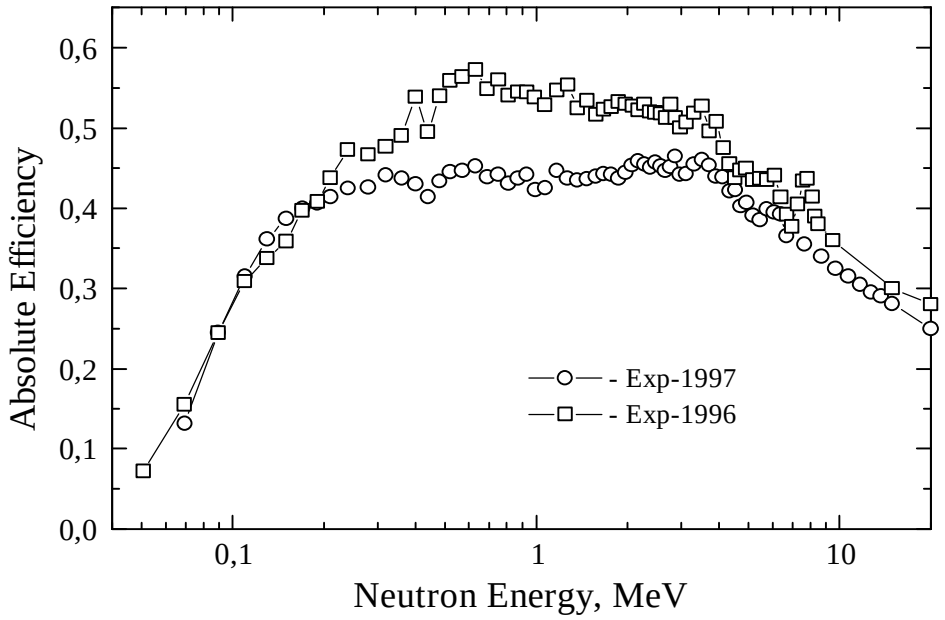

Fig. 4. Neutron detector efficiency, measured in experiments held in 1996 and 1997.

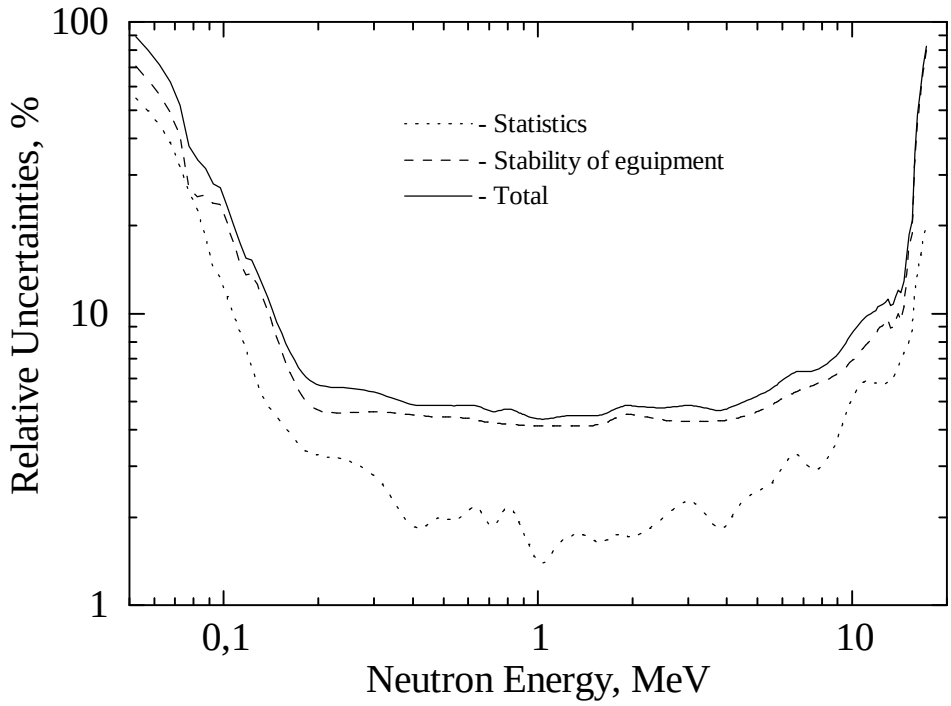

Fig. 5. Energy dependence of the total and component uncertainties of the leakage spectra from vanadium sphere 1.

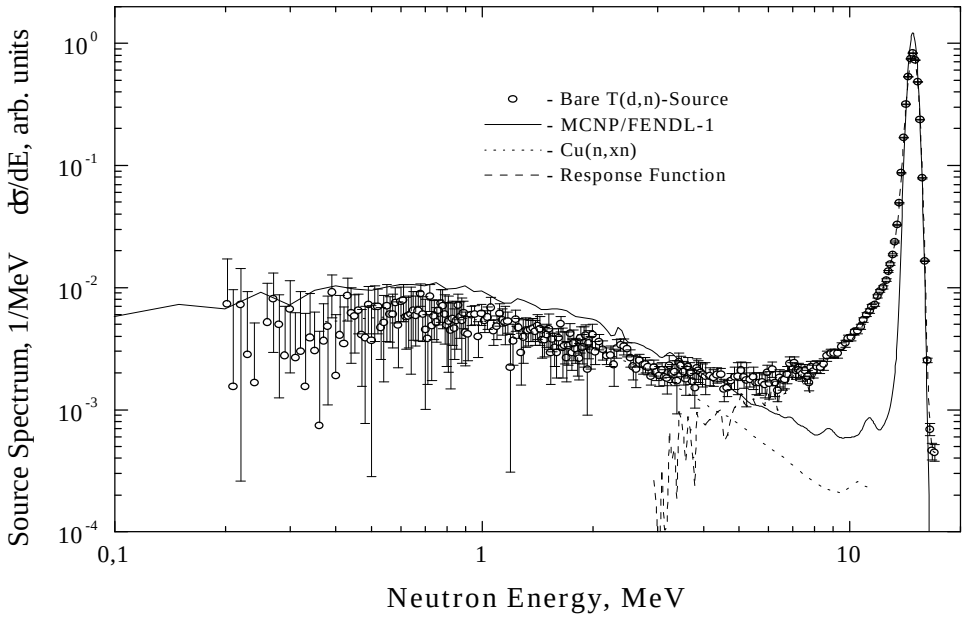

Fig. 6. Energy distribution of T(d,n) source neutrons, measured (points) and calculated (solid curve) at 8 degrees relative to incident deuteron beam. Dotted line - energy distribution of the secondary neutrons from C(n,xn) reaction. Dashed curve - spectrometer response function.

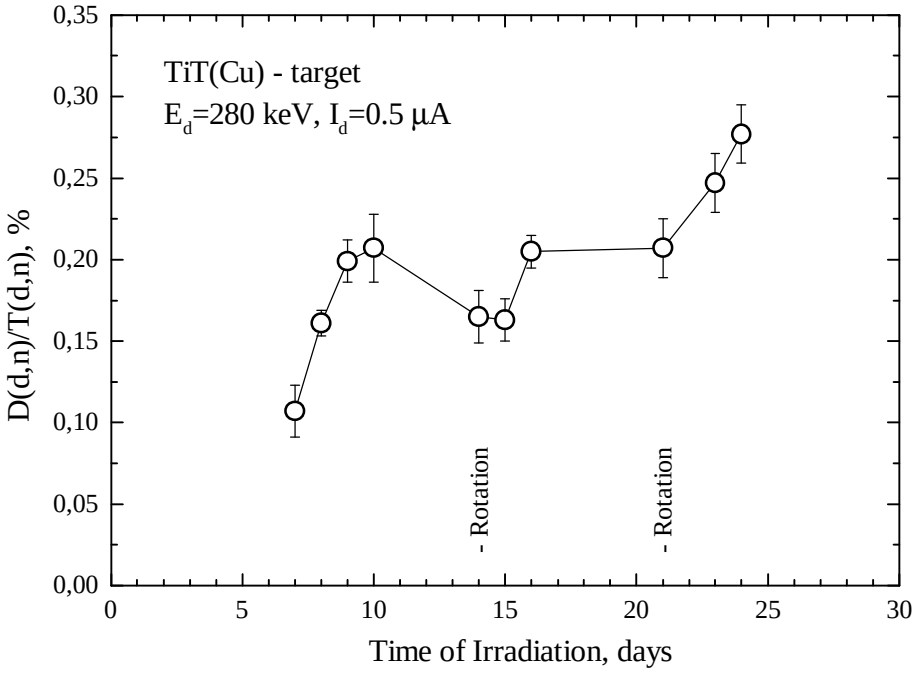

Fig. 7. The ratio of neutron yields from D(d,n) and T(d,n) reactions as a function of irradiation time („Rotation“ denotes the day of target rotation).

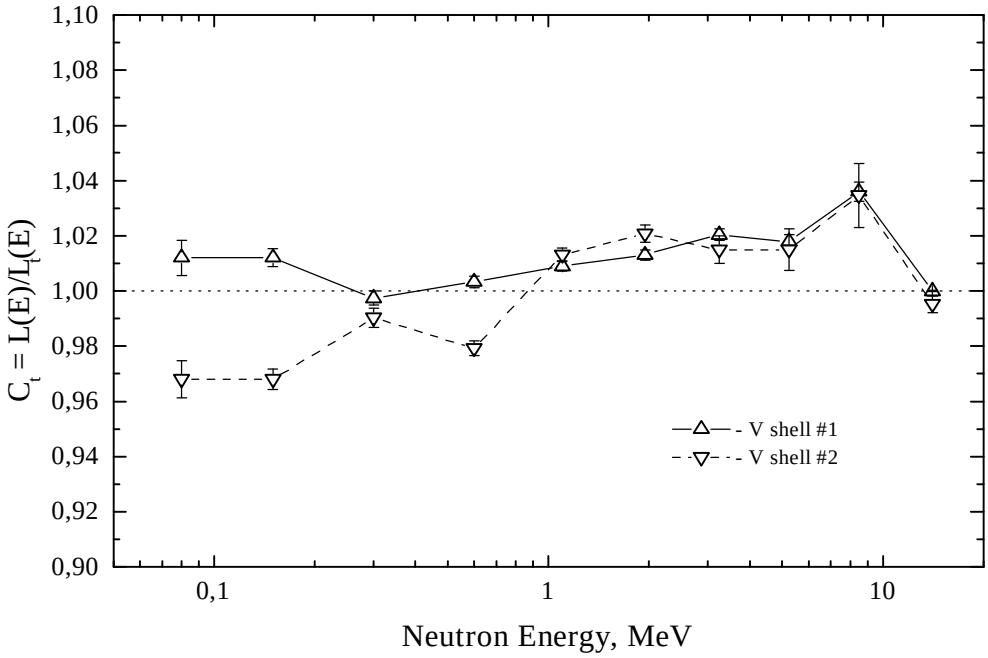

Fig. 8. Correction C_t for time-of-flight measuring technique.

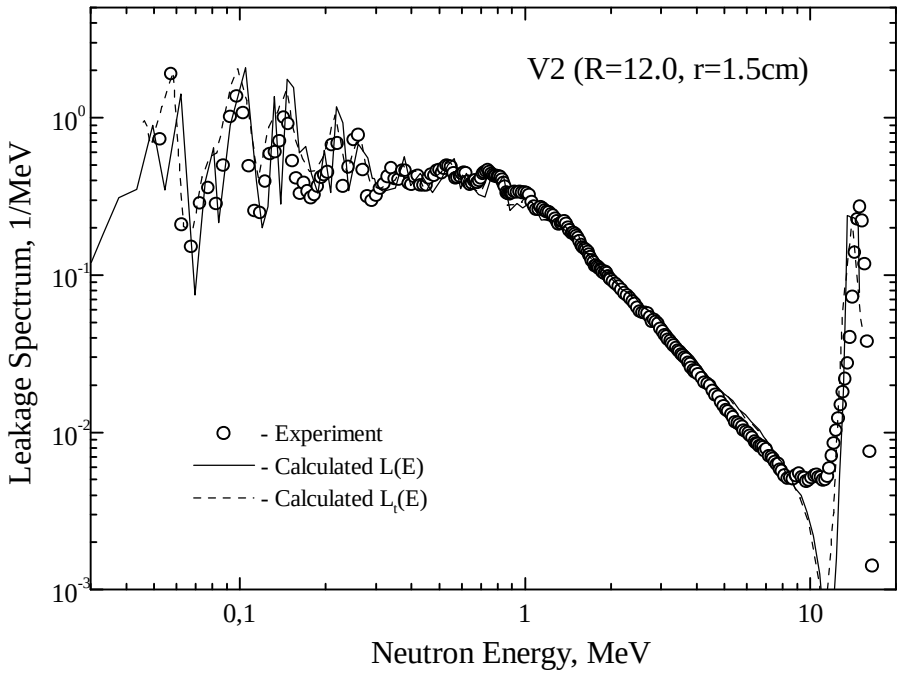

Fig. 9. Comparison of time dependent $L_t(E)$ and time and indepent $L(E)$ calculations of leakage spectra with experimental one for vanadium shell #2.

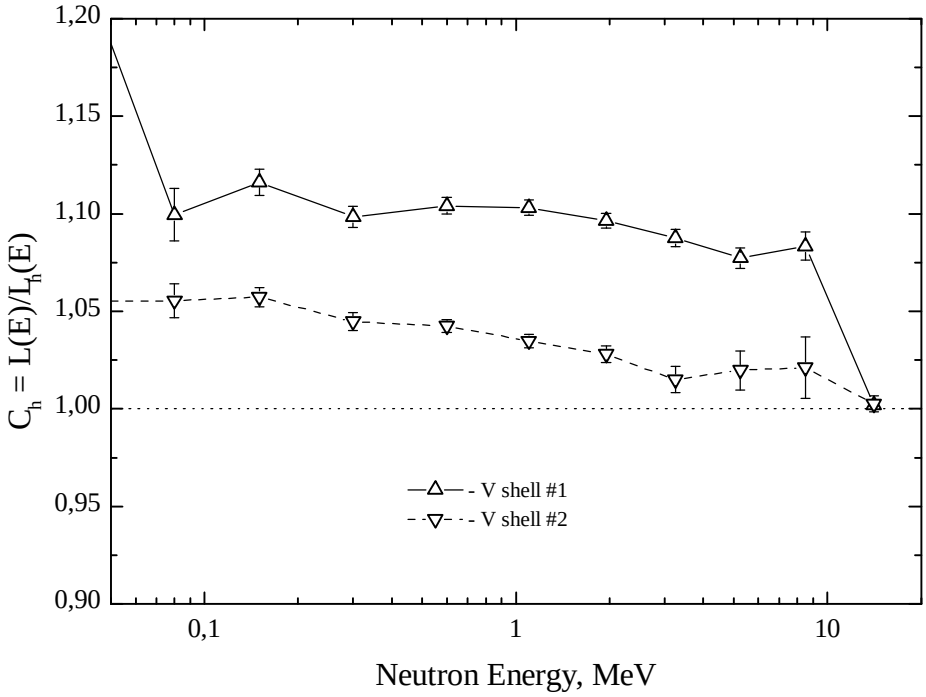

Fig. 10. Correction C_h for beam hole in shells.

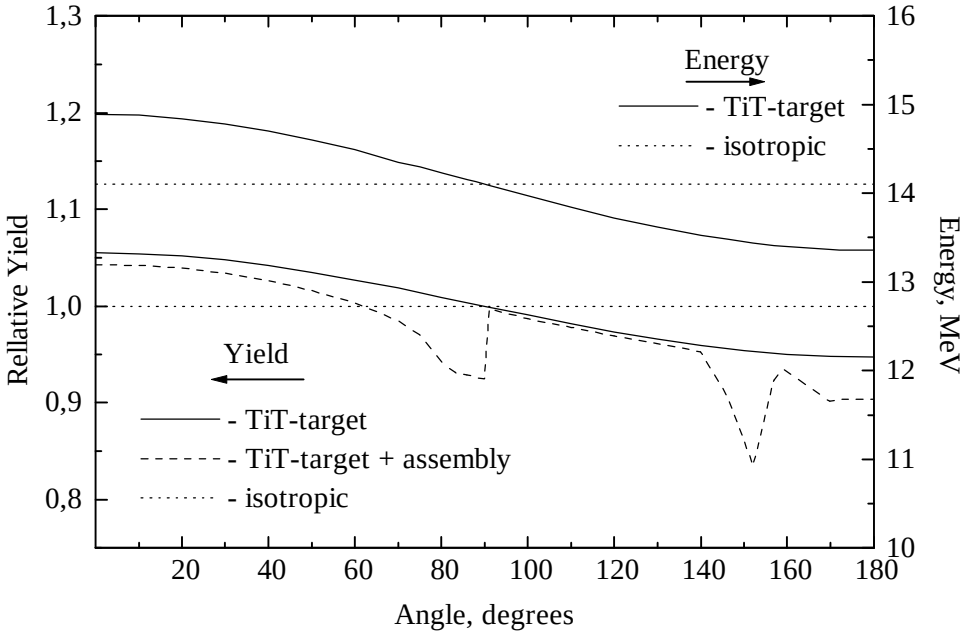

Fig. 11. Angular and energy distributions of '14-MeV' neutrons in the laboratory coordinate frame ('TiT - target' refers to a thick titanium-tritium target with an incident 280-keV deuteron beam).

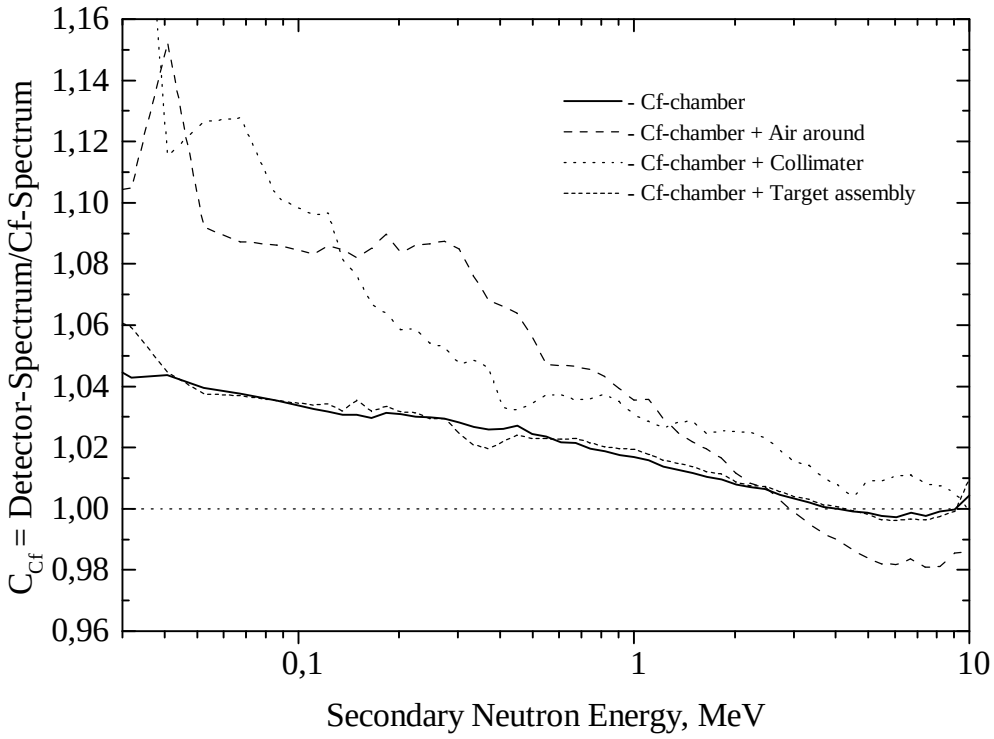

Fig. 12. Influence of the fission chamber, air, collimator and target assembly on ^{252}Cf spectrum.

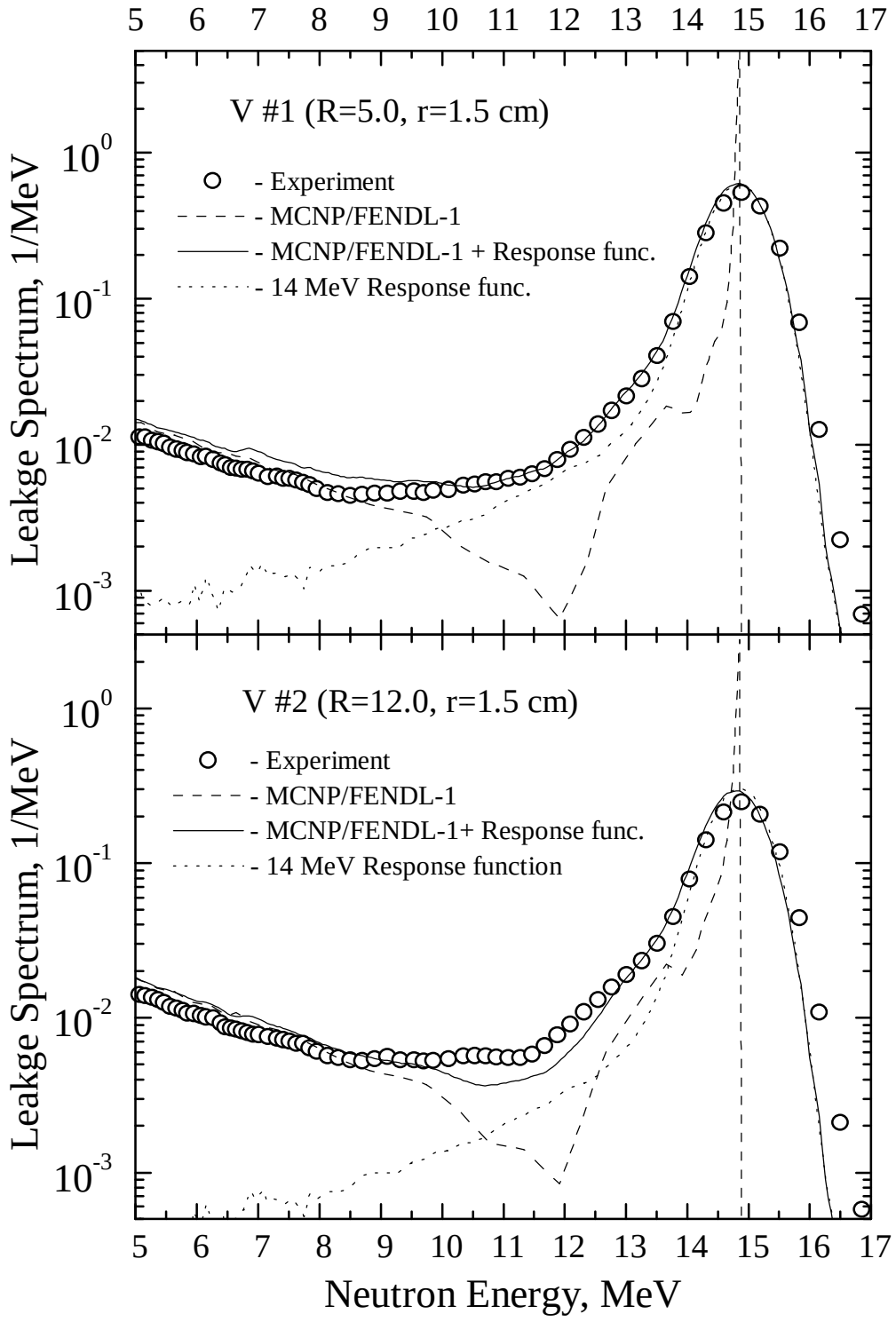

Fig. 13. Comparison of experimental (points) and calculated neutron leakage spectra before (dashed curve) and after (solid) folding calculated spectrum with the spectrometer response function (dotted) for two vanadium sphere #1 (top) and #2 (bottom).

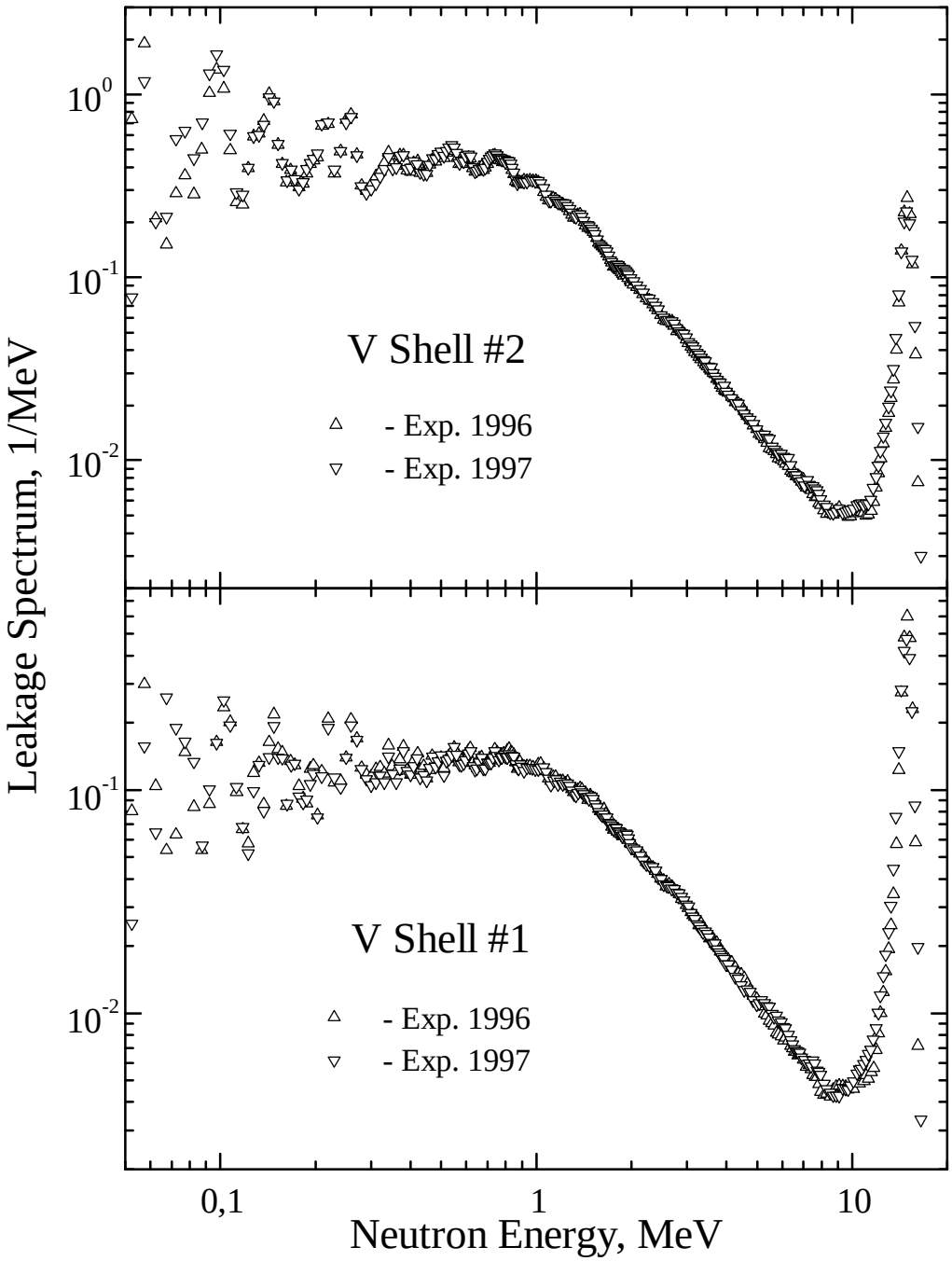

Fig. 14. Comparison of neutron leakage spectra, measured in 1996 and 1997.

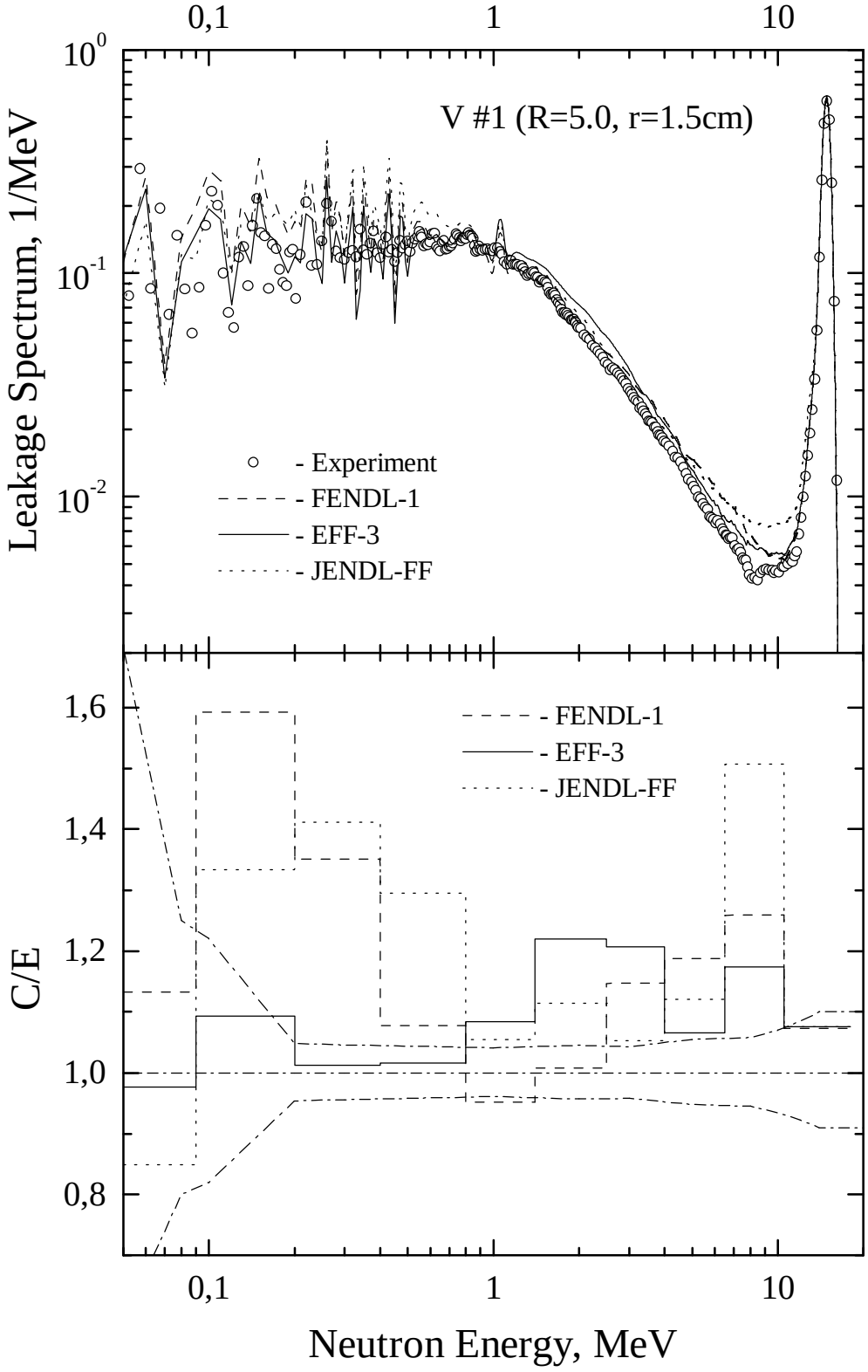

Fig. 15. Comparison of experimental and calculated neutron leakage spectra (top) and ratio C/E (bottom) for vanadium sphere #1. Dash-dotted curve denotes the experimental uncertainty corridor.

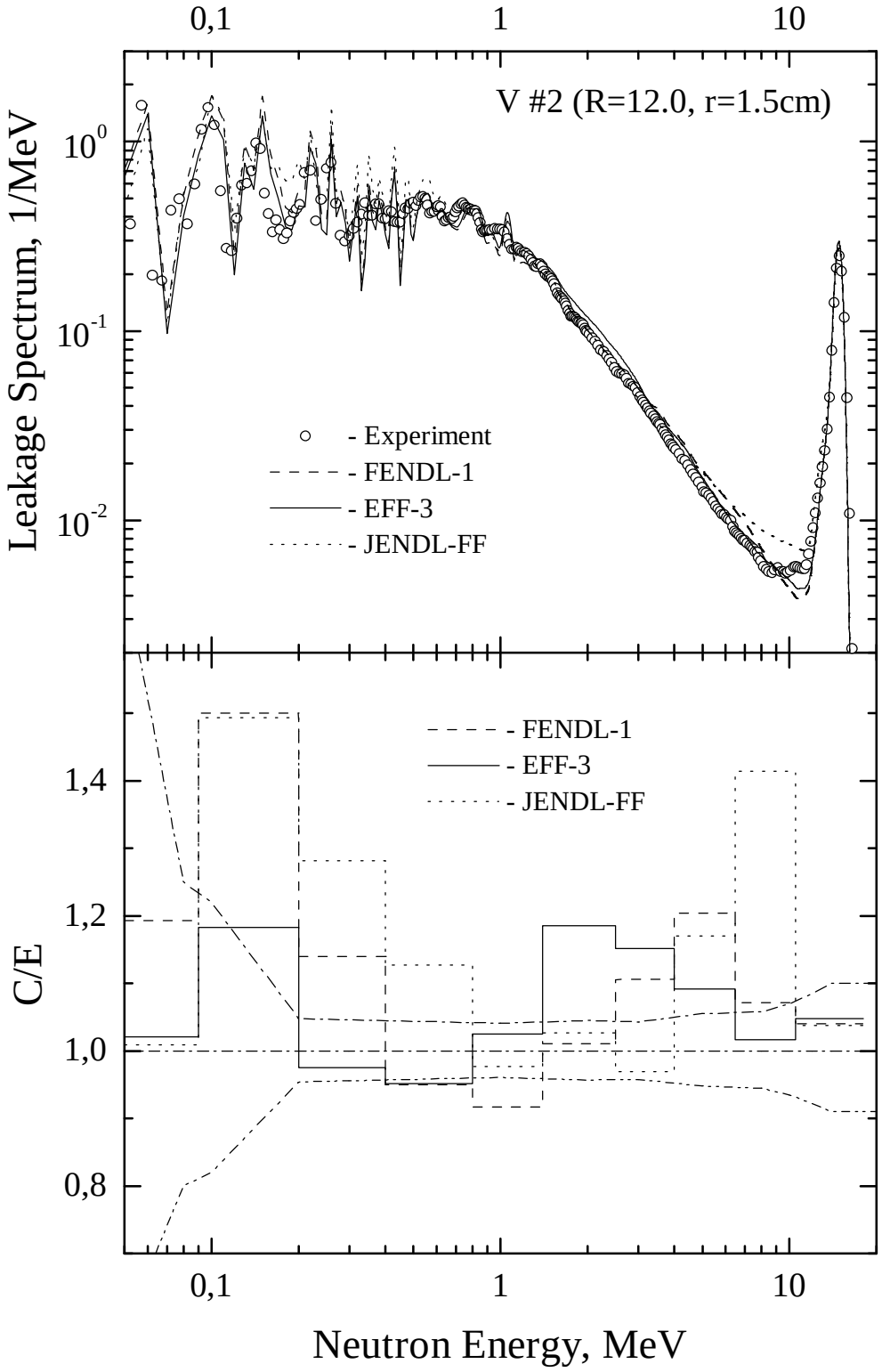

Fig. 16. Comparison of experimental and calculated neutron leakage spectra (top) and ratio C/E (bottom) for vanadium sphere #2. Dash-dotted curve denotes the experimental uncertainty corridor.

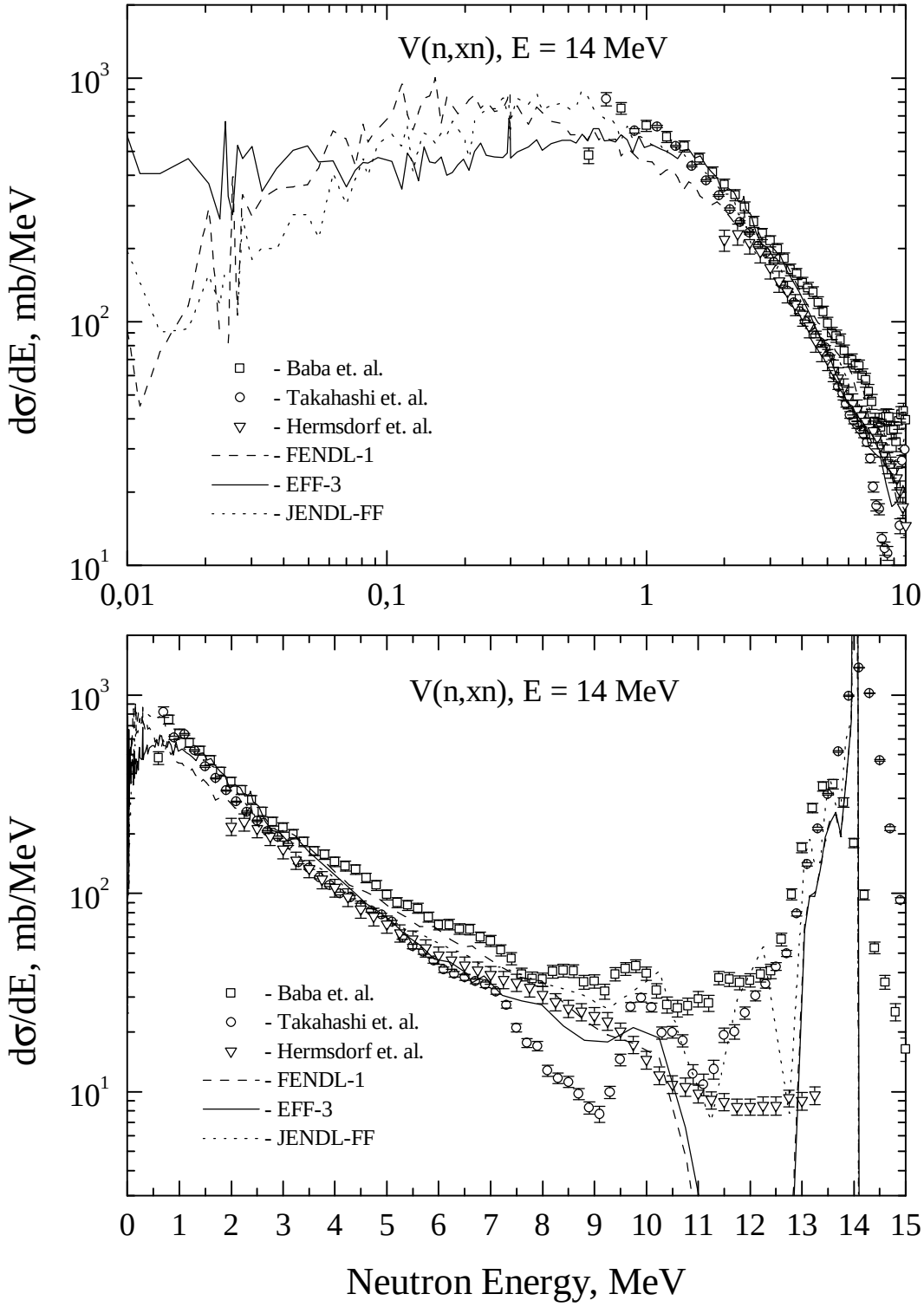

Fig. 17. Differential neutron emission cross section for V(n,xn) reaction at 14 MeV incident energy. Experimental data: squares - Baba et al. [15], circles - Takahashi et al. [17], down triangles - Hermsdorf et al. [16]. Evaluated data: dashed curve - FENDL-1, solid - EFF-3.0, dotted - JENDL-FF.